frontiers | Frontiers in Astronomy and Space Sciences

TYPE Original Research
PUBLISHED 06 May 2024
DOI 10.3389/fspas.2024.1381764

OPEN ACCESS

EDITED BY
Jaroslav Chum,
Institute of Atmospheric Physics (ASCR), Czechia

REVIEWED BY
David R. Shklyar,
Space Research Institute (RAS), Russia
Ashley Greeley,
National Aeronautics and Space Administration, United States

*CORRESPONDENCE
Chaoling Tang,
tcl@sdu.edu.cn

RECEIVED 04 February 2024
ACCEPTED 17 April 2024
PUBLISHED 06 May 2024

CITATION
Chen J, Tang C and Chu X (2024), The effect of continuous geomagnetic storms on enhancements of ultrarelativistic electrons in the Earth's outer radiation belt.
Front. Astron. Space Sci. 11:1381764.
doi: 10.3389/fspas.2024.1381764

The effect of continuous geomagnetic storms on enhancements of ultrarelativistic electrons in the Earth's outer radiation belt

Jingrun Chen[1,2], Chaoling Tang[1,2,3]* and Xinxin Chu[1]

[1]School of Space Science and Physics, Shandong University, Weihai, China, [2]National Space Science Center, State Key Laboratory of Space Weather, Chinese Academy of Sciences, Beijing, China, [3]Shandong Provincial Key Laboratory of Optical Astronomy and Solar-Terrestrial Environment, Institute of Space Sciences, Shandong University, Weihai, China

Ultrarelativistic electrons (E_k > 3 MeV) are the most energetic electrons in the Earth's outer radiation belt, which can cause serious damage to equipments on satellites. The evolutions of ultrarelativistic electrons during geomagnetic storm have been well understood, but the effects of continuous geomagnetic storm on ultrarelativistic electrons are still unclear. Using the data of the Van Allen Probes, we study the evolutions of ultrarelativistic electrons in the Earth's outer radiation belt during the three continuous geomagnetic storm events. These continuous geomagnetic storm events include the two geomagnetic storms. During the recovery phase of the first geomagnetic storm, enhanced relativistic and ultrarelativistic electrons with lower energies (≥ 3.4 MeV) are observed. These enhanced relativistic electrons could be the source of ultrarelativistic electrons and contribute to ultrarelativistic electron acceleration during the second geomagnetic storm. While 3.4 MeV electrons could be further enhanced during the second geomagnetic storm. During the recovery phase of the second small or moderate geomagnetic storm, ultrarelativistic electrons with higher cutoff energies (≥ 5.2 MeV) and higher fluxes are observed. Compared to an isolated geomagnetic storm with similar solar wind and geomagnetic conditions, ultrarelativistic electrons with higher cutoff energies and higher fluxes are observed during the recovery phase of the second geomagnetic storm. We also find that continuous geomagnetic storm events may contribute even more to enhancements of ultrarelativistic electrons in the outer radiation belt if the second geomagnetic storm is a small or moderate storm with a low solar wind dynamic pressure and short-duration main phase. These can help us to further understand the evolutions of ultrarelativistic electrons in the Earth's outer radiation belt during geomagnetic storms.

KEYWORDS

ultrarelativistic electrons, relativistic electrons, the outer radiation belt, continuous magnetic storms, flux loss and enhancement

1 Introduction

The Earth's outer radiation belt is occupied by electrons of a broad energy range (10 s keV—a few MeV). The extreme and rapid variations of the electrons of different energies during geomagnetic storms are observed due to different loss and acceleration mechanisms (e.g., Reeves et al., 2003; Chen et al., 2023; Wang et al., 2023). During the storm main phase, large depletions of the outer radiation belt electrons are usually observed. The adiabatic and nonadiabatic effects can contribute to the depletion of different energy electrons. The nonadiabatic effects mainly include 1) magnetopause shadowing and subsequent enhanced outward radial transport and 2) the scattering into the atmospheric loss cone due to wave-particle interaction. The magnetopause shadowing effect involves the loss of trapped electrons due to enhanced solar wind dynamic pressure. Subsequently, outward radial transport can lead to further loss of the outer radiation belt electrons (e.g., Kim et al., 2008; L. Y; Li et al., 2013; Loto'aniu et al., 2010; Shprits et al., 2006; Shprits et al., 2012; Turner et al., 2012; Ukhorskiy and Sitnov, 2008; Xiang et al., 2016; Yuan and Zong, 2013). Atmospheric precipitation of different energetic electrons in the outer radiation belt is due to resonant wave-particle interactions between different magnetospheric plasma waves and electrons. Previous studies have shown that electromagnetic ion cyclotron (EMIC) waves can scatter relativistic and ultrarelativistic electrons with small pitch angles and cause relativistic and ultrarelativistic electron precipitations (e.g., Carson et al., 2013; Clilverd et al., 2015; Engebretson et al., 2015; Kersten et al., 2014; L. Y; Li et al., 2016; Mourenas et al., 2016; Miyoshi et al., 2008; Ni et al., 2015). Yahnin et al. (2017) showed that of the more than a thousand relativistic electron precipitation events they counted, a quarter could be related to EMIC wave scattering. Xiang et al. (2018) showed that a combination of EMIC wave scattering and outward radial diffusion was the dominant dropout mechanism at high L^* region, while EMIC wave scattering could lead to dropouts at low L^*.

Usually, the fluxes of relativistic and ultrarelativistic electrons in the outer radiation belt can increase during the storm recovery phase due to the *DST* effect and different acceleration processes. Previous studies have shown an important role of local acceleration in ultrarelativistic electrons in the outer radiation belt (e.g., Reeves et al., 2013; Thorne et al., 2013; Li et al., 2014; Ma et al., 2016). Based on the Van Allen Probes data, Allison and Shprits, (2020) demonstrated that ultrarelativistic electrons could be locally accelerated up to 7 MeV by chorus waves. Allison et al. (2021) and Shprits et al. (2022) have also shown that the low plasma number density (−10 cm^{-3}) is a preferential condition for the local acceleration of ultrarelativistic electrons. Recently, Hua et al. (2022) revealed the natural upper limit of electron acceleration by chorus waves, which strongly depends on the lower energy boundary and the stable seed population.

Inward radial diffusion driven by ultralow-frequency (ULF) waves is also an important acceleration mechanism for ultrarelativistic electrons in the outer radiation belt (e.g., Reeves et al., 2013; Su et al., 2015). Jaynes et al. (2018) showed that the inward radial diffusion driven by ULF waves could account for enhancements of ultrarelativistic electrons. Zhao et al. (2018) showed that local acceleration could explain the flux enhancements for ~ 3–5 MeV electrons and the inward radial diffusion could contribute to the flux enhancements of −7 MeV electrons at the heart of the outer radiation belt during a small to moderate geomagnetic storm event. For the 17 March 2013 and 17 March 2015 geomagnetic storm events, the observed and simulation results have shown that the combined effect of local acceleration and inward radial diffusion could explain enhancements of ultrarelativistic electrons in the outer radiation belt (Baker et al., 2014; Li et al., 2016).

Many previous studies have focused on the effect of the solar wind and magnetospheric processes on relativistic electrons in the Earth's outer radiation belt (e.g., Drozdov et al., 2019; Forsyth et al., 2016; Gu et al., 2020; Kim et al., 2015; L. Y; Li et al., 2009; Reeves, 1998; Reeves et al., 2003; Reeves et al., 2011; Schiller et al., 2014; Su et al., 2014; Tang et al., 2016; Tang et al., 2017; Tang et al., 2023a.; Tang et al., 2023b; Turner et al., 2015; Turner et al., 2019; Wing et al., 2016; Zhao et al., 2017). Using the Van Allen Probes data, Li et al. (2015) have shown that high solar wind speed, prolonged southward interplanetary magnetic field (IMF) B_z component, and low solar wind dynamic pressure are critical for the electron (μ = 3,433 MeV/G) acceleration in the outer radiation belt. Using the data from the Relativistic Electron-Proton Telescope (REPT) instruments, Moya et al. (2017) statistically studied the effect of geomagnetic storms on the fluxes of ~ 2–5 MeV electrons in the outer radiation belt. They showed that the electron flux variations (enhancement, loss, and no change) mainly depended on *L*-shell and energy. Zhao et al. (2019a) studied the effects of solar wind conditions and geomagnetic storms on ultrarelativistic electron flux enhancements. They suggested that geomagnetic storms with higher solar wind speed, prolonged southward IMF B_z, higher solar wind E_y, lower solar wind number density, and continuous and intense substorm activities could contribute to enhancements of ultrarelativistic electrons in the outer radiation belt. Using the Van Allen Probes data, Chen et al. (2023) statistically studied the acceleration conditions of ultrarelativistic electrons with different cutoff energies in the outer radiation belt during geomagnetic storms. They found that different solar wind speeds and substorm activities during the recovery stage could cause enhancements of ultrarelativistic electrons with different energies.

Previous studies have focused on the evolution and acceleration conditions of ultrarelativistic electrons during isolated geomagnetic storms. However, the role of successive geomagnetic storms is not well understood. In this study, we will analyze the evolution of ultrarelativistic electrons in the outer radiation belt during the three typical continuous geomagnetic storm events, and discuss the effect of the first geomagnetic storm on the acceleration of ultrarelativistic electrons during the second geomagnetic storm.

2 Observations and analysis

Continuous magnetic storms in this study are defined as follows: 1) Each continuous magnetic storm event consists of two magnetic storms that are consecutive in time. Each continuous magnetic storm event lasts for a maximum of 2 weeks. The 2 weeks are the maximum time from the first SYM-Hmin to the end of the second storm recovery phase; 2) The enhancement of relativistic and ultrarelativistic electron flux occurs in the first magnetic storm; These enhanced fluxes are not significantly reduced until the second magnetic storm occurs. There are three typical continuous

geomagnetic storm events in this study. The reasons for these three events as typical events are as follows: 1) The second storm of these events was the small or moderate magnetic storm with a short main phase and low solar wind dynamic pressure; 2) The May 2013 event consisted of two successive moderate magnetic storms, which together led to enhancements of ultrarelativistic electrons; 3) The June 2013 event consisted of a strong magnetic storm (the first magnetic storm) and a moderate magnetic storm (the second magnetic storm), which together resulted in increased levels of ultrarelativistic electrons; 4) The April 2017 event consisted of two small magnetic storms, which together led to enhancements of >7 MeV electrons.

2.1 The May 2013 event

Figure 1 shows the first continuous geomagnetic storm event that occurred in May 2013. Solar wind parameters and geomagnetic indices with a time resolution of 1 min and level 2 spin average differential electron flux data from the Magnetic Electron Ion Spectrometer (MagEIS) (Blake et al., 2013) and REPT (Baker et al., 2012) instruments of the high energy particle, composition, and thermal plasma (ECT) suite (Spence et al., 2013) from the Van Allen Probes are used in the event analysis. Our study primarily uses the data from Van Allen Probe B. However, the data from Van Allen Probe A will be used when there are missing data for Van Allen Probe B. The fluxes of 1 MeV electrons are from the MagEIS, while the fluxes of >2 MeV electrons are from the REPT. This continuous magnetic storm event included a moderate geomagnetic storm on 18 May 2013 and a moderate geomagnetic storm on 25 May 2013. The geomagnetic storm on 18 May 2013 was caused by a halo CME accompanied by a flare of the magnitude ×1.2 (not shown). The minimum of the *SYM-H* index for this storm was −67 nT. In the recovery phase (the *SYM-H* index gradually returned from the $SYM\text{-}H_{\min}$ to −0 nT, which may last 4 days), the IMF B_z component fluctuated greatly in the north-south direction, and the minimum of the B_z component was about −10 nT (Figure 1G). The maximum solar wind speed was less than 500 km/s, and there were no solar wind high-speed flows (Figure 1H). The solar wind electric field E_y component had some perturbations (Figure 1I). In the early recovery phase (from 12:00 UT on 18 May to 00:00 UT on 20 May), two isolated weak substorms with the $AE_{\max}$ > 500 nT occurred. During the late recovery phase (from 00:00 UT on 20 May to 08:00 UT on 22 May), some small substorms with the $AE_{\max}$ < 700 nT appeared (Figure 1J). During the main phase (the *SYM-H* index rapidly declined from −0 nT to the $SYM\text{-}H_{\min}$, which may last 12 h), the fluxes of 1.0–5.2 MeV electrons significantly decreased based on the observations from Van Allen Probe B (Figures 1C–F). Xiang et al. (2018) have showed that the dominant dropout mechanisms at high L^* region are often a combination of EMIC wave scattering and outward radial diffusion. At the same time, the solar wind dynamic pressure was up to 9 nPa (not shown), which can compress the magnetospause and lead to the electron flux loss (e.g., Hudson et al., 2014; Gao et al., 2015; Gokani et al., 2022). At ~ 02:54–03:03 UT on 18 May 2013, Van Allen Probe B was located at duskside and observed some EMIC waves at three bands (H^+, He^+ and O^+) at L^* ~ 4.0 (SI, Supplementary Figure S1). Meredith et al. (2003) combined satellite observations with theoretical results to suggest that EMIC waves interact primarily with electrons above MeV energies. Lei et al. (2023) showed that three bands of EMIC waves (H^+, He^+ and O^+) have a stronger scattering effect on electrons at higher L. These guggested that the EMIC wave scattering make some contribution for the decreased fluxes. The decrease in electron flux may also have other causes. During the recovery phase, enhanced fluxes of 1.0–3.4 MeV electrons were observed at L^* ~ 4.4 (Figures 1D–F), which may be due to local acceleration (e.g., Thorne et al., 2013). The peak flux of 1 MeV electrons appeared at L^* ~ 4.4 at ~ 14:36 UT on 20 May 2013, and the flux was 692 cm^{-2}/s/sr/keV. The peak flux of 3.4 MeV electrons appeared at L^* ~ 4.3 at ~ 06:46 UT on 22 May 2013, and the flux was 1850 cm^{-2}/s/sr/MeV. In this event, the flux of 5.2 MeV electrons did not enhance (Figure 1C). According to the definition of Chen et al. (2023), this storm event was defined as an event with a cutoff energy of 3.4 MeV event (Figures 1A–F).

The second moderate geomagnetic storm occurred on 25 May 2013, about 7 days after the first geomagnetic storm, and was caused by a halo CME (not shown). The minimum of the *SYM-H* index was −65 nT. During the main phase (from 18:00 UT on 24 May to 05:00 UT on 25 May) and the early stage of the recovery phase (from 05:00 UT on 25 May to 00:00 UT on 27 May), the B_z and E_y components had strong perturbations (Figures 1G,I). The solar wind velocity started to increase and reached 770 km/s (Figure 1H). The continuous substorm activities occurred, and the AE^*_{max} was up to 1,423 nT (Figure 1J). From the observations of Van Allen Probe B, the fluxes of 1 MeV and 3.4 MeV electrons during the main phase did not significantly decrease (Figures 1E,F). This may be related to the intensity of the geomagnetic storm, the duration of the main phase, and the lower dynamic pressure of the solar wind, which we will discuss in detail in the discussion section. During the recovery phase (from 05:00 UT on 25 May to 00:00 UT on 30 May), the fluxes of 1.0, 2.1, 3.4, and 5.2 MeV electrons gradually began to increase (Figures 1A–F). The peak flux of 1.0 MeV electrons appeared at L^* ~ 4.8 at ~ 14:50 UT on 29 May 2013, and the flux was 1,566 cm^{-2}/s/sr/keV (Figure 1F). The maximum energy of ultrarelativistic electrons with the flux enhancements during the recovery phase was 6.3 MeV, and its peak flux appeared at L^* ~ 4.7 at ~14:53 UT on 29 May 2013 (Figure 1A). The growing local peaks in the electron phase space densities (PSDs) for μ = 1,096, 2,290, 3,311, 4,786, 6,918, and 8,317 MeV/G were observed (SI, Supplementary Figure S2). Many previous studies have suggested that the rising local peaks of the electron PSD are caused by local acceleration due to the wave-particle resonance interaction between chorus waves and electrons (e.g., Reeves et al., 2013; Thorne et al., 2013; W; Li et al., 2014; Ma et al., 2016; Hua, Bortnik, and Ma, 2022). Thus, enhancements of ultrarelativistic electrons were mainly due to the local acceleration by chorus waves.

Figure 2 shows the variations of the electron fluxes with different energies at L^* ~ 4.5 during the first continuous geomagnetic storm event in May 2013. L^* ~ 4.5 was the main acceleration region of radiation belt electrons. The flux values were taken for each pass of Van Allen Probe B through the main acceleration region of ultrarelativistic electrons. Some values of the observations from Van Allen Probe B are bad points, which are blanked out in Figure 2. When the flux value at a given moment is 0 or −1.00000E+31, which is much lower than the fluxes at nearby moment, we refer

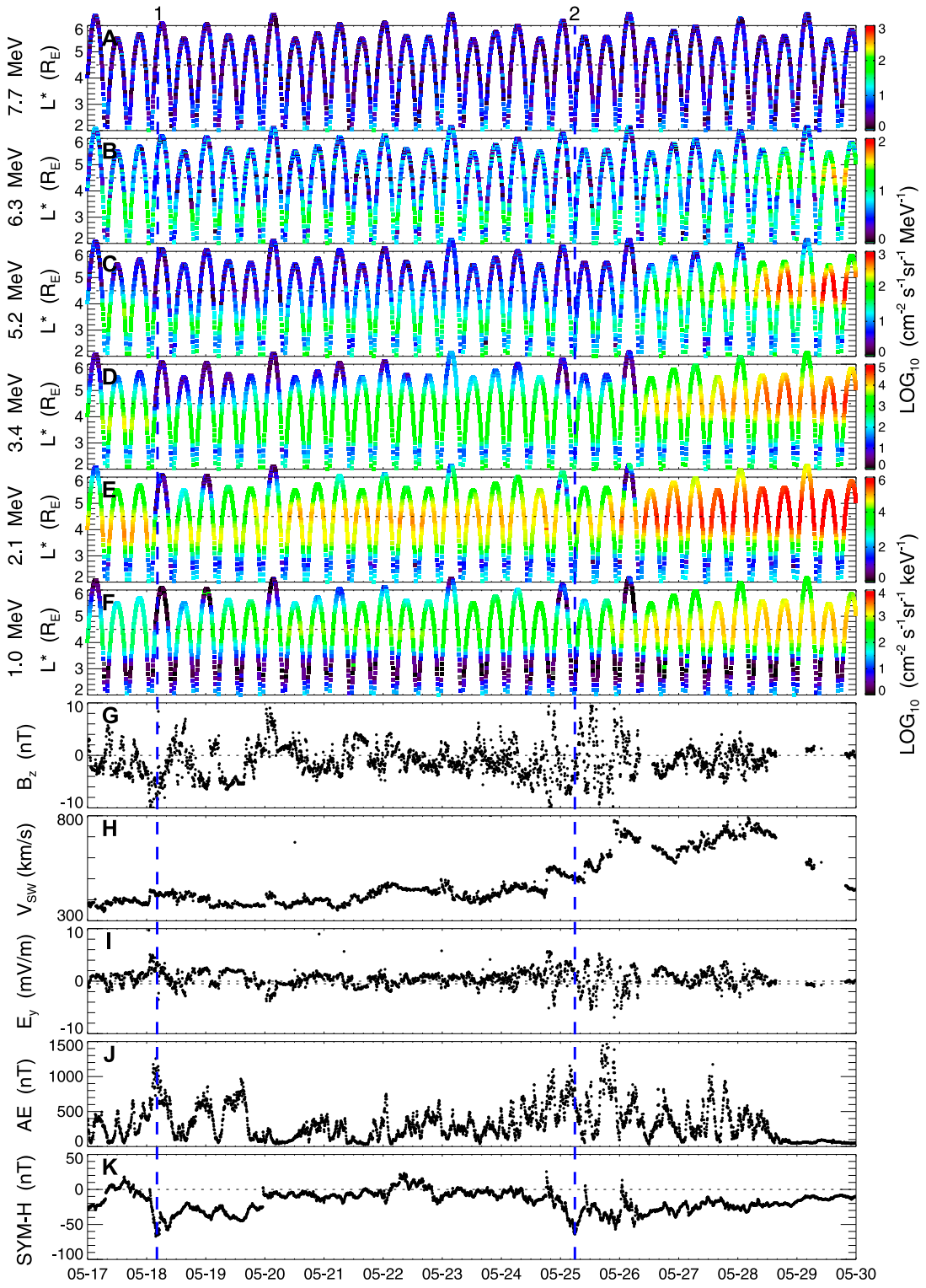

FIGURE 1
An overview of the first continuous geomagnetic storm event that occurred in May 2013. The cutoff energy of the geomagnetic storm on 18 May 2013 is 3.4 MeV, while that of the geomagnetic storm on 25 May 2013 is 6.3 MeV. Panels **(A–F)** show the electron fluxes at energies of 7.7 MeV, 6.3 MeV, 5.2 MeV, 3.4 MeV, 2.1 MeV, and 1.0 MeV, respectively. The black dotted lines in **(A–F)** represent the $L*$ value of the flux enhancements of ultrarelativistic electrons at different energies during the second geomagnetic storm (L^* ~ 4.5). Panels **(G–K)** show the IMF B_z, solar wind velocity V_{sw}, and solar wind electric field E_y in the GSM coordinates, *AE* index, and the *SYM-H* index, respectively. L^* is the calculated Roederer's shell parameter (in units of the radius of the Earth), for which the internal magnetic field (IGRF) and external (OP77Q) models are used. The vertical blue dashed lines indicate the times of the *SYM-H*$_{min}$ during the first continuous geomagnetic storm event.

to the data at that moment as a bad point. For the data with fluxes less than 10^1/cm^2/s/sr/MeV (instrument background noise), they may be affected by background levels and galactic cosmic rays (e.g., Zhao et al., 2019b). There were some small flux perturbations during Van Allen Probe B pass, which may be due to the Dst effect. The cutoff energy of the geomagnetic storm on 25 May 2013 was 6.3 MeV. During the first geomagnetic storm, the flux of 1.0 MeV electrons (F_1) decreased from 6.8 × 10^4 cm^{-2}/s/sr/MeV to 7.4 × 10^3 cm^{-2}/s/sr/MeV and then increased to 5.5 × 10^5 cm^{-2}/s/sr/MeV during the recovery phase. Before the main phase of the second geomagnetic storm, F_1 was 3.3 × 10^5 cm^{-2}/s/sr/MeV, which had some losses compared with the flux peak of the first geomagnetic storm. Then, F_1 decreased to 1.2 × 10^5 cm^{-2}/s/sr/MeV during the main phase of the second geomagnetic storm. In the recovery phase of the second geomagnetic storm, F_1 increased to 1.4 × 10^6 cm^{-2}/s/sr/MeV. Compared to F_1 during the main phase of the first geomagnetic storm, F_1 during the main phase of the second geomagnetic storm increased by nearly one order of magnitude. These enhanced relativistic electrons could be used as the source of ultrarelativistic electrons and contribute to ultrarelativistic electron acceleration during the second geomagnetic storm (e.g., Allison et al., 2021; Chen et al., 2023; W; Li et al., 2014; Shprits et al., 2022; Thorne et al., 2013). The fluxes of 3.4 MeV electrons (F_2) decreased to 6.2 cm^{-2}/s/sr/MeV during the main phase of the first geomagnetic storm and increased to 754 cm^{-2}/s/sr/MeV during the late recovery phase of the first geomagnetic storm. Then, F_2 decreased to 117 cm^{-2}/s/sr/MeV during the main phase of the second geomagnetic storm, and the flux peak of F_2 during the recovery phase of the second geomagnetic storm was 3.0 × 10^4 cm^{-2}/s/sr/MeV. Compared to F_2 during the recovery phases of the first continuous geomagnetic storm event, the fluxes of 3.4 MeV electrons were further enhanced during the second geomagnetic storm. And, enhanced fluxes of 5.2 and 6.3 MeV electrons were observed during the second geomagnetic storm.

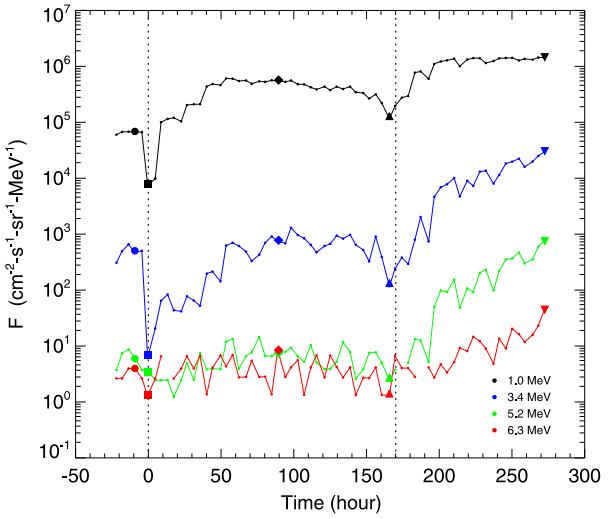

FIGURE 2
Variations in the electron fluxes with different energies at L^* ~ 4.5 during the first continuous geomagnetic storm event in May 2013. Energies are distinguished by colors. Black, blue, green, and red represent 1.0 MeV, 3.4 MeV, 5.2 MeV, and 6.3 MeV, respectively. The symbols represent the sequences of storm events, in turn, before the first geomagnetic storm (at ~ 18:38 UT on 17 May 2013) (circle), the later main phase of the first geomagnetic storm (at ~ 03:27 UT on 18 May 2013) (square), the later recovery phase of the first geomagnetic storm (at ~ 21:46 UT on 21 May 2013) (diamond), the later main phase of the second geomagnetic storm (at ~ 03:18 UT on 25 May 2013) (upward triangle) and the later recovery phase of the second geomagnetic storm (at ~ 15:07 on 29 May 2013) (downward triangle). The dotted line on the left indicates the time of the *SYM-H*$_{min}$ of the first geomagnetic storm (at ~ 03:40 UT on 18 May 2013), and the dotted line on the right indicates the time of the *SYM-H*$_{min}$ of the second geomagnetic storm (at ~ 05:46 UT on 25 May 2013).

2.2 The June 2013 event

Figure 3 shows the second continuous geomagnetic storm that occurred in June 2013. The continuous geomagnetic storm event included a strong geomagnetic storm on 1 June 2013 and a moderate geomagnetic storm on 7 June 2013. The minimum *SYM-H* index for the storm on 1 June 2013 was −137 nT. During the storm main phase (from 00:00 UT to 12:00 UT on 1 June), there was a strong IMF B_z component, which was up to −21 nT (Figure 3G). The solar wind speed was about 400 km/s (Figure 3H). The maximum solar wind electric field E_y component was 8.64 mV/m (Figure 3I). There was an isolated strong substorm and AE^*_{max} reached 1,391 nT (Figure 3J). In the recovery phase (from 12:00 UT on 1 June to 12:00 UT on 6 June), the B_z component had some perturbations in the north-south direction (Figure 3G). The long-duration high-speed flows appeared, and the peak of the solar wind speed was up to 775 km/s (Figure 3H). The E_y component also had some perturbations (Figure 3I), and some continuous weak substorm activities occurred (Figure 3J). The decreased fluxes of relativistic and ultrarelativistic electrons during the storm main phase were observed by Van Allen probe B (Figures 3B–F). Some EMIC waves were also observed by Van Allen Probe B at ~ 05:50–06:10 UT on 1 June 2013 (SI, Supplementary Figure S3). This suggested that EMIC wave scattering possibly contributed to the reduction in the fluxes of relativistic and ultrarelativistic electrons (e.g., Turner et al., 2014; Xiang et al., 2018). In the recovery phase, the accelerated relativistic and ultrarelativistic electrons were observed at L^* ~ 4.0–4.6 (Figures 3C–F). The peak flux of 1 MeV electrons appeared at L^* ~ 4.3 at ~ 12:42 UT on 3 June 2013, and the flux was 1,369 cm^{-2}/s/sr/keV (Figure 3F). In this event, the maximum electron energy during the recovery phase was 5.2 MeV. The peak flux of 5.2 MeV electrons was 97 cm^{-2}/s/sr/MeV, which appeared at L^* ~ 4.6 at ~ 18:38 UT on 5 June 2013 (Figure 3C).

The second geomagnetic storm occurred on 7 June 2013, about 6 days after the first geomagnetic storm. The minimum *SYM-H* index was −88 nT. During the main phase (from 16:00 UT on 6 June to 04:00 UT on 7 June 2013) and the early stage of the recovery phase (from 04:00 UT on 7 June to 12:00 UT on 8 June), the B_z component was southward and lasted about 1 day (Figure 3G). The maximum solar wind speed was less than 500 km/s (Figure 3H), and the E_y component was less than 6 mV/m (Figure 3I). The continuous substorm activities occurred, and AE^*_{max} was 1,347 nT (Figure 3J). From the observations of Van Allen probe B, the fluxes of relativistic and ultrarelativistic electrons during the storm main phase were not significantly decreased (Figures 3C–F). During the recovery phase (from 04:00 UT on 7 June to 00:00 UT on 11 June), the

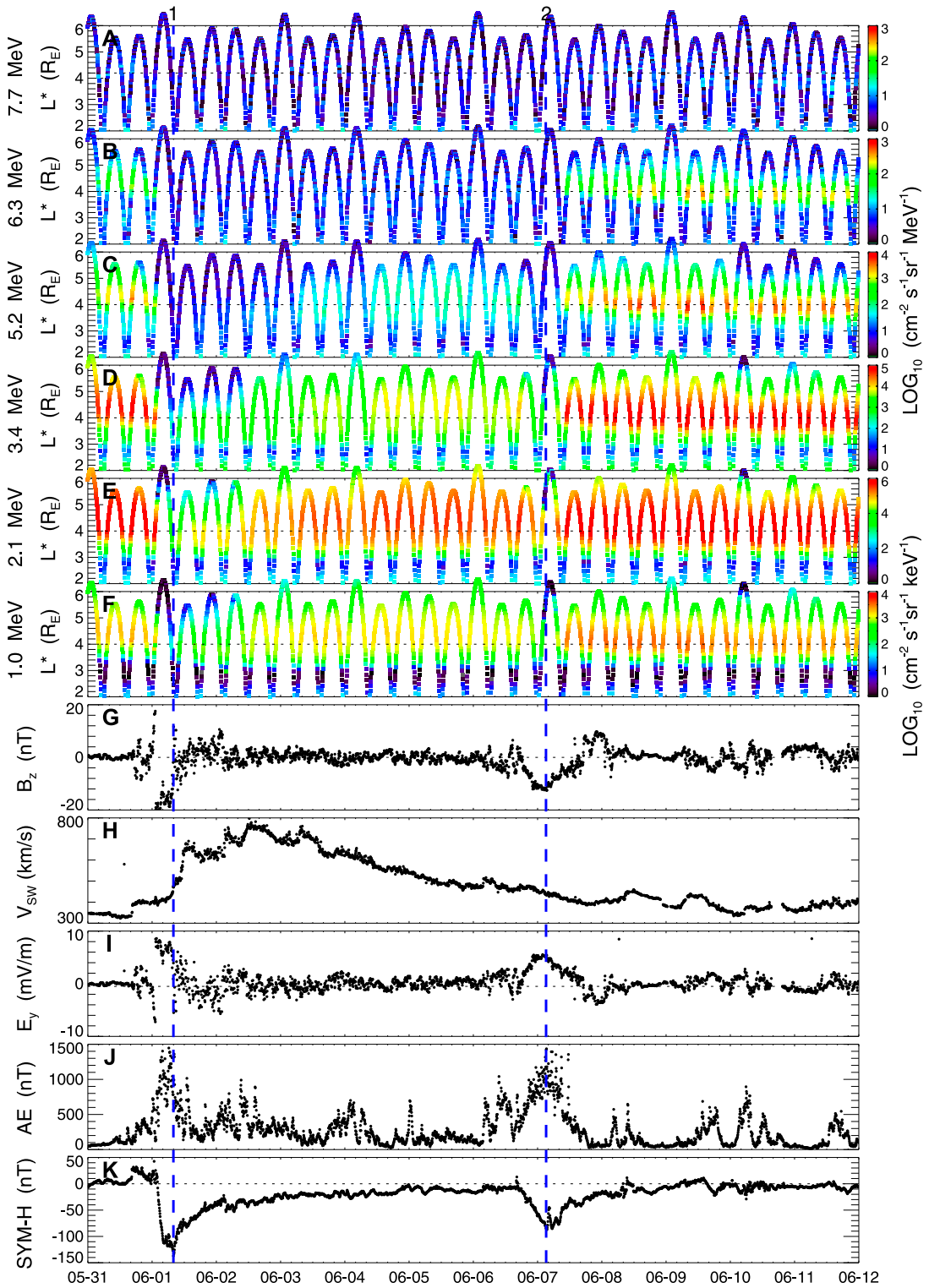

FIGURE 3
An overview of the second continuous geomagnetic storm event that occurred in June 2013. The cutoff energy of the geomagnetic storm event on 1 June 2013 is 3.4 MeV, while that of the geomagnetic storm event on 7 June 2013 is 6.3 MeV. Panels **(A–F)** show the electron fluxes at energies of 7.7 MeV, 6.3 MeV, 5.2 MeV, 3.4 MeV, 2.1 MeV, and 1.0 MeV, respectively. The black dotted lines in **(A–F)** represent the $L*$ value of the flux enhancements of ultrarelativistic electrons at different energies during the second geomagnetic storm (L^* ~ 4.0). Panels **(G–K)** show the IMF B_z, solar wind velocity V_{sw}, and solar wind electric field E_y in the GSM coordinates, *AE* index, and the *SYM-H* index, respectively. The vertical blue dashed lines indicate the times of the *SYM-H*$_{min}$ during the second continuous geomagnetic storm event.

fluxes of 1.0–6.3 MeV electrons recovered and enhanced rapidly. The peak flux of 1.0 MeV electrons appeared at L^* ~ 4.0 at ~ 10:25 UT on 8 June 2013, the flux was 2.9 × 10^3 cm^{-2}/s/sr/keV (Figure 3F). The maximum energy of ultrarelativistic electrons was 6.3 MeV. The peak flux of 6.3 MeV electrons was 371 cm^{-2}/s/sr/MeV and appeared at L^* ~ 3.9 at ~ 07:50 UT on 9 June 2013 (Figure 3B). The features of inward radial diffusion in the electron PSDs for μ = 1,096, 2,290, 3,311, 4,786, 6,918, and 8,317 MeV/G were observed (SI, Supplementary Figure S4), which indicated that the inward radial diffusion could contribute to enhancements of ultrarelativistic electrons at L^* ~ 4.0.

Figure 4 shows the variations of the electron fluxes with different energies at L^* ~ 4.0 during the second continuous geomagnetic storm event in June 2013. L^* ~ 4.0 was the main acceleration region of ultrarelativistic electrons during the second geomagnetic storm. The cutoff energy of the geomagnetic storm on 7 June 2013 was 6.3 MeV. Before the first geomagnetic storm on 1 June 2013, 1.0 MeV, 3.4 MeV, 5.2 MeV, and 6.3 MeV electrons had higher fluxes based on the observations from Van Allen Probe B (as shown by the circles in Figure 4). During the later main phase of the first geomagnetic storm, the fluxes of relativistic and ultrarelativistic electrons significantly decreased, their fluxes were 3.0 × 10^4 cm^{-2}/s/sr/MeV, 83 cm^{-2}/s/sr/MeV, 1 cm^{-2}/s/sr/MeV, and 4 cm^{-2}/s/sr/MeV for 1.0 MeV, 3.4 MeV, 5.2 MeV, and 6.3 MeV electrons, respectively (as shown by the squares in Figure 4). The fluxes of 1.0 MeV, 3.4 MeV, and 5.2 MeV electrons during the recovery phase of the first geomagnetic storm increased to 9.0 × 10^5 cm^{-2}/s/sr/MeV, 3.8 × 10^3 cm^{-2}/s/sr/MeV, and 55 cm^{-2}/s/sr/MeV, respectively (as shown by the diamonds in Figure 4). During the main phase of the second geomagnetic storm, the fluxes of 1.0 MeV, 3.4 MeV, and 5.2 MeV electrons decreased slightly (as shown by the upward triangles in Figure 4). Finally, enhanced fluxes of ultrarelativistic electrons were observed during the recovery phase of the second geomagnetic storm (as shown by the downward triangles in Figure 4).

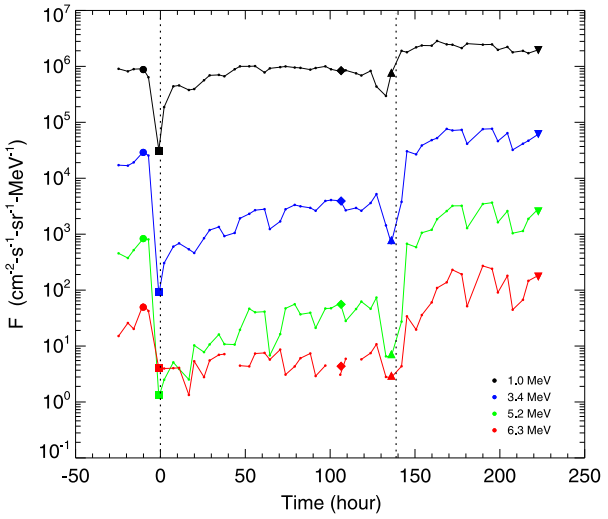

FIGURE 4
Variations in the electron fluxes with different energies at L^* ~ 4.0 during the second continuous geomagnetic storm in June 2013. The symbols represent the sequences of storm events, in turn, before the first geomagnetic storm (at ~ 21:51 UT on 31 May 2013) (circle), the later main phase of the first geomagnetic storm (at ~ 07:11 UT on 1 June 2013) (square), the later recovery phase of the first geomagnetic storm (at ~ 19:09 UT on 5 June 2013) (diamond), the later main phase of the second geomagnetic storm (at ~ 01:27 UT on 7 June 2013) (upward triangle) and the later recovery phase of the second geomagnetic storm (at ~ 16:28 UT on 10 June 2013) (downward triangle). The dotted line on the left indicates the time of the *SYM-H*$_{min}$ of the first geomagnetic storm (at ~ 07:48 UT on 1 June 2013), and the dotted line on the right indicates the time of the *SYM-H*$_{min}$ of the second geomagnetic storm (at ~ 02:41 UT on 7 June 2013).

2.3 The April 2017 event

Figure 5 shows the third continuous geomagnetic storm event that occurred in April 2017. Data of the electron fluxes is from both Van Allen Probe A and B. This continuous geomagnetic storm event included a small geomagnetic storm on 20 April 2017 and a small geomagnetic storm on 22 April 2017. The minimum *SYM-H* index of the geomagnetic storm on 20 April 2017 was −48 nT. During the main phase (from 00:00 UT on 20 April to 05:00 UT on 20 April), the southward IMF B_z component was about −12 nT (Figure 5G), the maximum solar wind speed was about 550 km/s (Figure 5H), and the maximum solar wind electric field E_y component was 6 mV/m (Figure 5I). According to the observations of Van Allen probe B, the fluxes of 3.4 MeV and 1 MeV electrons began to decrease at 00:00 UT on 20 April 2017 (Figures 5E,F). During the recovery phase (from 05:00 UT on 20 April to 14:00 UT on 21 April), the IMF B_z component had some fluctuations in the north-south direction (Figure 5G). There were long-duration high-speed flows of the solar wind, and the peak velocity of the solar wind was up to 600 km/s (Figure 5H). The E_y component had some perturbations (Figure 5I). The intense substorm activities occurred, and the AE^*_{max} reached 1,135 nT (Figure 5J). The fluxes of 1.0–3.4 MeV electrons had no significant decreases during the main phase but increased during the recovery phase (Figures 5D–F). The peak flux of 1 MeV electrons was 907 cm^{-2}/s/sr/keV, which appeared at L^* ~ 4.5 at 15:49 UT on 21 April 2017. In this event, the maximum energy of enhanced electrons during the recovery phase was 3.6 MeV and the peak flux was 2,730 cm^{-2}/s/sr/keV, which appeared at L^* ~ 3.6 at ~ 09:58 UT on 21 April 2017.

The minimum *SYM-H* index of the small geomagnetic storm on 22 April was −53 nT, which was caused by the halo CME associated with C5.5 flares (not shown). During this geomagnetic storm, the B_z component had some fluctuations in the north-south direction (Figure 5G). There were long-duration high-speed flows, and the peak solar wind speed reached 767 km/s (Figure 5H). The E_y component had also some fluctuations (Figure 5I). The continuous and intense substorm activities occurred during the recovery phase (from 04:00 UT on 22 April to 00:00 UT on 26 April), and the AE^*_{max} reached 1,290 nT (Figure 5J). Chen et al. (2023) have shown that continuous intense substorms in the early recovery stage are important to the rapid recovery and enhancements of ultrarelativistic electrons in the outer radiation belt. These conditions may be favorable for enhancements of 7.7 MeV electrons. Note that there are ~7 h of the missing data from Van Allen Probe B on April 22. However, when combined with the observations from Van Allen Probe A, the evolution of relativistic and ultrarelativistic electrons was similar to the first two storm events. That is, the

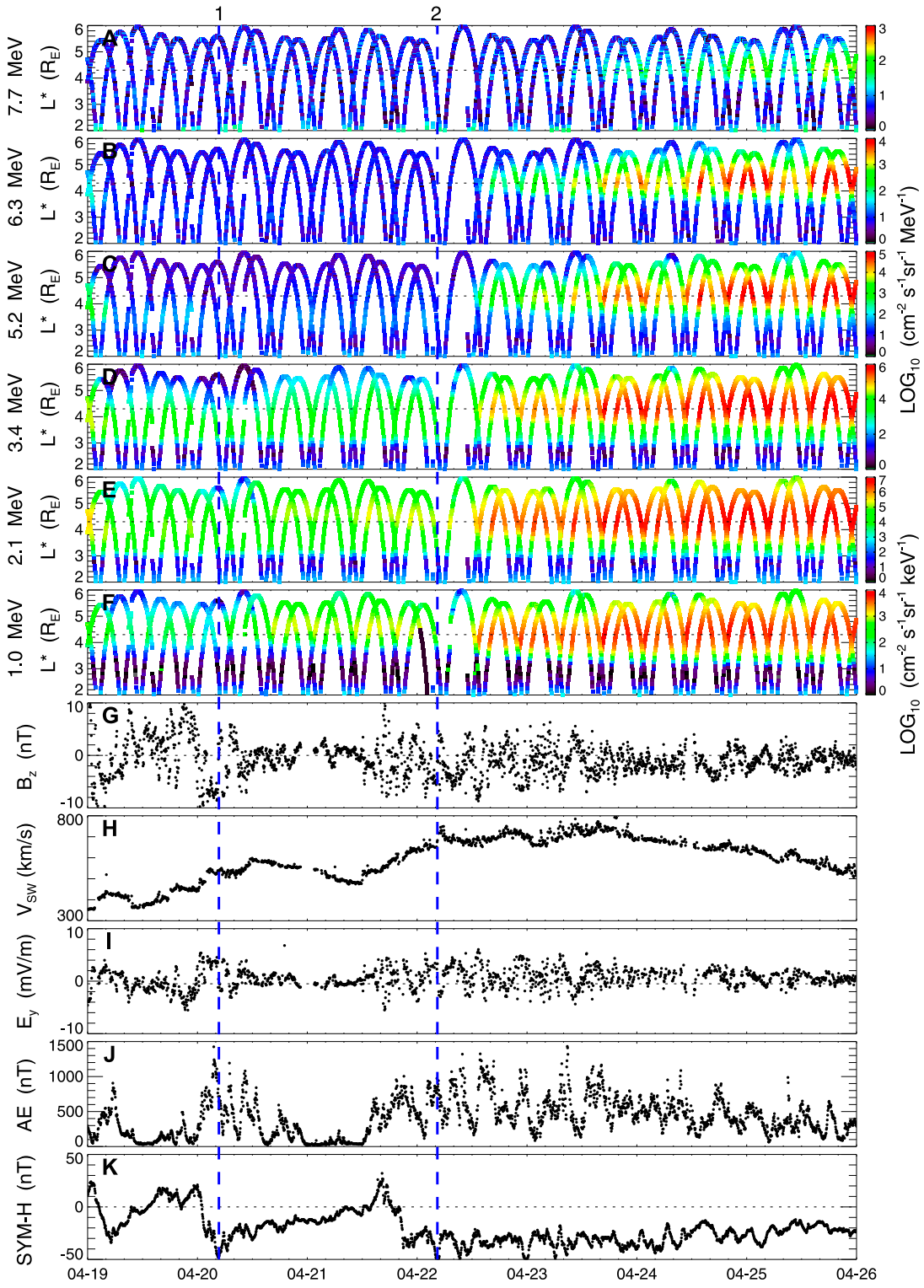

FIGURE 5
An overview of the third continuous geomagnetic storm event that occurred in April 2017. The cutoff energy of the geomagnetic storm event on 20 April 2017 is 3.4 MeV, while that of the geomagnetic storm event on 22 April 2017 is 6.3 MeV. Panels **(A–F)** show the electron flux at energies of 7.7 MeV, 6.3 MeV, 5.2 MeV, 3.4 MeV, 2.1 MeV, and 1.0 MeV, respectively. The black dotted lines in **(A–F)** represent the $L*$ value of the flux enhancements of ultrarelativistic electrons at different energies during the second geomagnetic storm ($L^* \sim 4.3$). Panels **(G–K)** show the IMF B_z, solar wind velocity V_{sw}, and solar wind electric field E_y in the GSM coordinates, *AE* index, and the *SYM-H* index, respectively. The vertical blue dashed lines indicate the times of the $SYM\text{-}H_{min}$ during the third continuous geomagnetic storm event. Data is from Van Allen Probe A and B

fluxes of relativistic and ultrarelativistic electrons during the storm main phase were not significantly decreased. The fluxes of 3.4, 5.2, and 6.3 MeV electrons started to increase during the early recovery phase (from 04:00 UT on 22 April to 08:00 UT on 23 April). The peak fluxes of 3.4, 5.2, and 6.3 MeV electrons appeared at L^* ~ 4.3 (Figures 5B–D). The peak flux of 3.4 MeV electrons was 5.5 × 10^5 cm^{-2}/s/sr/MeV, which appeared at 14:11 UT on 25 April 2017. The peak flux of 1 MeV electrons was 5.0 × 10^3 cm^{-2}/s/sr/keV, which appeared at L^* ~ 4.3 at 16:50 UT on 23 April 2017. The maximum energy of ultrarelativistic electrons with the flux enhancements during the recovery phase was 7.7 MeV. The peak flux of 7.7 MeV electrons appeared at L^* ~ 4.4 at ~ 01:07 UT on 25 April 2017, and the flux was 237 cm^{-2}/s/sr/MeV.

Figure 6 shows the variations of the electron fluxes with different energies at L^* ~ 4.3 during the third continuous geomagnetic storm event in April 2017. L^* ~ 4.3 was the main acceleration region of ultrarelativistic electrons during the second geomagnetic storm. As from Figure 6, the fluxes of 1.0–6.3 MeV electrons first had some decreases during the main phase (as shown by the squares in Figure 6). EMIC wave scattering possibly contributed to the decreases (e.g., Turner et al., 2014; Su et al., 2016; Xiang et al., 2018). Because the intense EMIC waves were observed by Van Allen Probe B during the main phase (at ~ 03:07–03:33 UT on 20 April 2017) (SI, Supplementary Figure S5). Then the fluxes of 1.0–5.2 MeV electrons increased during the recovery phase of the first geomagnetic storm (as shown by the diamonds in Figure 6). During the main phase of the second geomagnetic storm, the fluxes of 1.0–5.2 MeV electrons continued to increase (as shown by the upward triangles in Figure 6). These enhanced 1 MeV electrons during the first geomagnetic storm could be the direct "source" of ultrarelativistic electrons and contributed to ultrarelativistic electron acceleration during the second geomagnetic storm. Ultrarelativistic electrons (3.4 MeV and 5.2 MeV electrons) during the first geomagnetic storm could be further enhanced during the second geomagnetic storm. Compared to the fluxes of ultrarelativistic electrons during the recovery phase of the first geomagnetic storm, the fluxes of 3.4 MeV electrons enhanced by two orders of magnitude, the fluxes of 5.2 MeV and 6.3 MeV electrons increased by three orders of magnitude, and the fluxes of 7.7 MeV electrons were also greatly enhanced during the recovery phase of the second geomagnetic storm (as shown by the downward triangles in Figure 6).

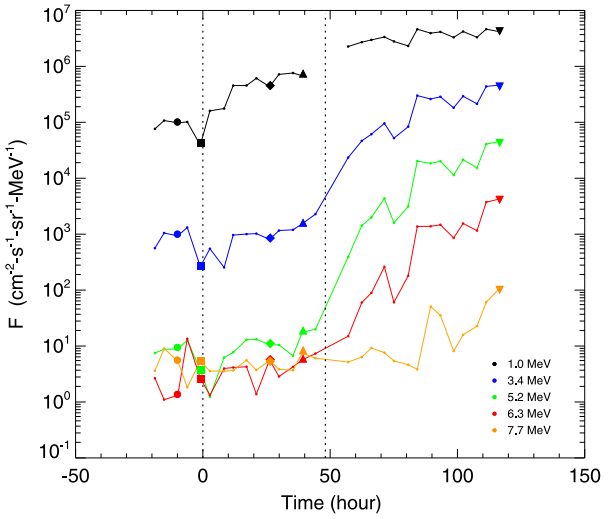

FIGURE 6
Variations in the electron fluxes with different energies at L^* ~ 4.3 during the third continuous geomagnetic storm in April 2017. The symbols represent the sequence of storm events, in turn, before the first geomagnetic storm (at ~ 18:39 UT on 19 April 2017) (circle), the later main phase of the first geomagnetic storm (at ~ 03:32 UT on 20 April 2017) (square), the later recovery phase of the first geomagnetic storm (at ~ 06:46 UT on 21 April 2017) (diamond), the later main phase of the second geomagnetic storm (at ~ 19:35 UT on 21 April 2017) (upward triangle) and the later recovery phase of the second geomagnetic storm (at ~ 01:14 UT on 25 April 2017) (downward triangle). The dotted line on the left indicates the time of the *SYM-H*$_{min}$ of the first geomagnetic storm (at ~ 04:28 UT on 20 April 2017), and the dotted line on the right indicates the time of *SYM-H*$_{min}$ of the second geomagnetic storm (at ~ 04:35UT on 22 April 2017).

3 Discussions

Previous studies have shown that high solar wind speed (V_{sw} > 500 km/s) and continuous substorms play an important role in the acceleration of ultrarelativistic electrons in the Earth's outer radiation belt (e.g., Baker et al., 1997; Baker et al., 2019; Hajra et al., 2015; Kim et al., 2015; W; Li et al., 2015; Zhao et al., 2019a). Using the data from Van Allen Probes, Chen et al. (2023) statistically studied 82 acceleration events of ultrarelativistic electrons in the outer radiation belt. They found that the acceleration of ultrarelativistic electrons at different energies requires the different solar wind speeds and different substorm activities. To further study the role of successive geomagnetic storms in the evolution or enhancements of ultrarelativistic electrons in the Earth's outer radiation belt, we compare some isolated geomagnetic storm events picked from Chen et al. (2023) to the second geomagnetic storms in the three typical continuous geomagnetic storm events.

The storm on 25 May 2013 was the second geomagnetic storm in the first continuous geomagnetic storm event in May 2013, and a selected similar event was the isolated geomagnetic storm on 5 August 2019. The intensity of the geomagnetic storm on 5 August 2019 was −64 nT. The long-duration high-speed flows appeared during the recovery phase and continuous substorms occurred during the early recovery phase (SI, Supplementary Figure S6). The two geomagnetic storms had similar solar wind speed flows, the evolution and intensity of storms, and substorm activities during the recovery phases. The cutoff energy of the geomagnetic storm on 5 August 2019 was 5.2 MeV, and the acceleration region was mainly at L^* ~ 4.8 (SI, Supplementary Figure S6), while the cutoff energy of the geomagnetic storm on 25 May 2013 was 6.3 MeV, and the acceleration region was mainly at L^* ~ 4.5 (Figure 1). Tang et al. (2023b) have shown that the timing, duration, and intensity of substorms during the storm recovery phase are crucial to the location of the local acceleration region. The electron fluxes of all energies during the recovery phase of the geomagnetic storm on 25 May 2013 were at least double those of the geomagnetic storm on 5 August 2019 (SI, Supplementary Figure S7). These results show that the moderate geomagnetic storm in this continuous geomagnetic

storm event has higher cutoff energy and higher flux levels than the isolated geomagnetic storm with similar conditions.

The storm on 7 June 2013 was the second geomagnetic storm in the second continuous geomagnetic storm event in June 2013, and a selected similar storm was the isolated geomagnetic storm on 27 August 2014. The $SYM\text{-}H_{\min}$ of the geomagnetic storm on 27 August 2014 was −90 nT (SI, Supplementary Figure S8). For the two geomagnetic storms, the solar wind speed flows and the evolution and intensity of storms were similar. The cutoff energy of the geomagnetic storm on 27 August 2014 was 5.2 MeV, and the acceleration region was mainly at L^* ~ 4.5 (SI, Supplementary Figure S8), while the cutoff energy of the geomagnetic storm on 7 June 2013 was 6.3 MeV, and the acceleration region was mainly at L^* ~ 4.0 (Figure 2). The flux levels of relativistic and ultrarelativistic electrons during the recovery phase of the geomagnetic storm on 7 June 2013 were much larger than those of the geomagnetic storm on 27 August 2014 (SI, Supplementary Figure S9). These results show that the moderate geomagnetic storm in this continuous geomagnetic storm events has higher cutoff energy and higher flux levels than the isolated geomagnetic storms with continuous substorm activities.

The storm on 22 April 2017 was the second geomagnetic storm in the third continuous geomagnetic storm event in April 2017, and a selected similar event was the geomagnetic storm on 31 January 2017. The intensity of the geomagnetic storm on 31 January 2017 was −48 nT (SI, Supplementary Figure S10). The two geomagnetic storms had similar solar wind speed flows, the evolution and intensity of storms, and continuous substorm activities during the recovery phases. The cutoff energy of the geomagnetic storm on 31 January 2017 was 6.3 MeV, and the acceleration region was mainly at L^* ~ 4.6 (SI, Supplementary Figure S10), while the cutoff energy of the geomagnetic storm on 22 April 2017 was 7.7 MeV, and the acceleration region was mainly at L^* ~ 4.3 (Figure 3). The flux levels of relativistic and ultrarelativistic electrons during the recovery phase of the geomagnetic storm on 22 April 2017 were much higher than those of the geomagnetic storm on 31 January 2017 (SI, Supplementary Figure S11). Chen et al. (2023) showed that the enhancement of ultrarelativistic electrons was related to continuous and intense substorms during the recovery phase of the geomagnetic storm. Our results suggest that continuous magnetic storms also can contribute to enhancements of ultrarelativistic electrons during the geomagnetic storm. And, Zhao et al. (2019a) showed that more intense geomagnetic storms were easy to lead to the flux enhancements of ultrarelativistic electrons with higher energies. However, ultrarelativistic electrons with higher cutoff energies (≥5.2 MeV) and higher fluxes are observed during the recovery phases of the second small or moderate geomagnetic storms.

Some factors may influence whether continuous geomagnetic storm events can affect the evolution and acceleration of ultrarelativistic electrons in the Earth's outer radiation belt. The first factor is solar wind dynamic pressure. Previous studies have shown that enhanced solar wind pressure can compress the magnetopause and lead to electron flux dropouts (e.g., Onsager et al., 2007; Turner et al., 2012; Yuan and Zong, 2013; Hudson et al., 2014; Gao et al., 2015; Xiang et al., 2016; Gokani et al., 2022). And, magnetospheric compressions can also lead to the anisotropic distributions of ions and electrons, which generate EMIC waves on the dayside (e.g., Anderson and Hamilton, 1993; McCollough et al., 2010; Usanova et al., 2012; Zhang et al., 2016b; Saikin et al., 2016; Xue et al., 2023; Yan et al., 2023) that can cause the loss of relativistic and ultrarelativistic electrons (e.g., Zhang et al., 2016a; Su et al., 2017; Zhu et al., 2020). Hua et al. (2023) found that the most significant flux losses of >1 MeV electrons occurred during the strong solar wind dynamic pressure while the flux losses barely occurred during the weak solar wind dynamic pressure. During the second geomagnetic storm of the three continuous geomagnetic storm events in this study, the solar wind dynamic pressures were relatively low or had only an instantaneous enhancement. Thus, the fluxes of relativistic and ultrarelativistic electrons in the outer radiation belt during the main phase were not significantly decreased.

The second factor is the intensity of the second geomagnetic storm of the continuous geomagnetic storm event. During the storm main phase, the large depletions of the outer radiation belt electrons were due to the Dst effect (Kim and Chan, 1997; Li et al., 1997) and nonadiabatic effects. Usually, the electron dropouts caused by the Dst effect are positively correlated with the intensity of geomagnetic storms. Xiang et al. (2018) have shown that the electron dropouts at higher L shells due to outward radial diffusion induced by magnetopause shadowing require stronger geomagnetic storms. Previous studies have shown that EMIC waves can cause relativistic and ultrarelativistic electron precipitations by scattering relativistic and ultrarelativistic electrons with small pitch angles (e.g., Shprits et al., 2013; 2016; Turner et al., 2014; Usanova et al., 2014; Rodger et al., 2015; Zhang et al., 2016a; 2016b; Su et al., 2016; Staples et al., 2023). Previous studies also have shown that the losses of relativistic and ultrarelativistic electrons caused by EMIC wave scattering at lower L shells are more likely to occur during geomagnetic storms (e.g., Zhang et al., 2016b; Xiang et al., 2018; Hua et al., 2023). In this study, the second geomagnetic storm of the three continuous geomagnetic storm events is small or moderate geomagnetic storm. Using the data from Van Allen Probe B, only some EMIC waves were observed at high L^* ($L^* > 5$) (not shown). Thus, the decreases of relativistic and ultrarelativistic electrons in the center of the outer radiation belt during the main phases of the second geomagnetic storms were smaller. These relativistic electrons could be used as the source of ultrarelativistic electrons and contribute to ultrarelativistic electron acceleration, while the fluxes of 3.4 MeV electrons were further enhanced during the second geomagnetic storm.

The third factor is the duration of the main phase. Wang et al. (2023) found that the duration of the main phase played an important role in the evolutions of the seed and MeV electrons in the outer radiation belt during geomagnetic storms. EMIC waves were important for the losses of ultrarelativistic electrons at lower L shells, which is associated with shorter time scales (e.g., Meredith et al., 2003; Summers et al., 2007; Cao et al., 2017; Ni et al., 2018). Previous studies have also shown that EMIC waves can drive sub-relativistic and relativistic electrons into the loss cone over a time scale of several hours (e.g., Ni et al., 2015; Yuan et al., 2018; Capannolo et al., 2019; Zhu et al., 2020; Zhang et al., 2021). These time scales were related to the intensity of EMIC waves. In this study, the durations of the storm main phases of the second geomagnetic storms were less than 12 h. Thus, the fluxes of 1.0 MeV and 3.4 MeV electrons did not decrease significantly during the short-duration main phases.

Furthermore, Yahnin and Yahnina (2022) studied two consecutive geomagnetic storms that formed under similar conditions, with a rapid decay of the relativistic electron flux during the main phase of the first magnetic storm but not during the main phase of the second. They explained that variations in the relativistic electron flux during the main phase of the second magnetic storm were related to relativistic electron acceleration. The $SYM\text{-}H_{min}$ of the second magnetic storm in their study was < -100 nT, and $AE_{max} > 1{,}500$ nT. The second magnetic storms in the three continuous magnetic storm events analyzed in this paper were small or moderate magnetic storms, and substorm activities during the main phase were not strong. Thus, the enhancement of the relativistic electron flux due to the strong geomagnetic perturbation is not the main factor for the absence of flux decay of the relativistic electron flux during the main phase of the second magnetic storm.

Of course, these are not the only factors that can influence the final flux levels. Some factors (e.g., high-speed flows of the solar wind and substorm activities during the second magnetic storm event, etc.) may also have an impact on the resulting the enhancement of electron fluxes. After all, the evolution of ultrarelativistic electrons in the outer radiation belts is a very complex process. Further statistical study of the "the effect of continuous magnetic storms events on ultra-relativistic electrons" is our future tasks.

4 Conclusion

In this work, we studied the evolution of ultrarelativistic electrons in the Earth's outer radiation belt during the three continuous geomagnetic storm events. Each continuous geomagnetic storm event included two magnetic storms. The main conclusions can be summarized as follows:

(1) During the recovery phase of the first geomagnetic storm, enhanced relativistic and ultrarelativistic electrons with lower energies (≥3.4 MeV) are observed. These enhanced relativistic electrons could be the source of ultrarelativistic electrons and contribute to ultrarelativistic electron acceleration during the second geomagnetic storm. While 3.4 MeV electrons could be further enhanced during the second geomagnetic
(2) During the recovery phase of the second small or moderate geomagnetic storm, ultrarelativistic electrons with higher cutoff energies (≥5.2 MeV) and higher fluxes are observed.
(3) Compared to isolated geomagnetic storms with similar solar wind and geomagnetic conditions, ultrarelativistic electrons with higher cutoff energies and higher fluxes are observed during the recovery phase of the second geomagnetic storm.
(4) If the second geomagnetic storm is a small or moderate storm with a low solar wind dynamic pressure and short-duration main phase, continuous geomagnetic storm events may contribute even more to enhancements of ultrarelativistic electrons in the outer radiation belt.

Data availability statement

The datasets presented in this study can be found in online repositories. The names of the repository/repositories and accession number(s) can be found in the article/Supplementary Material.

Author contributions

JC: Data curation, Investigation, Software, Writing–original draft. CT: Funding acquisition, Project administration, Supervision, Writing–review and editing. XC: Data curation, Writing–review and editing.

Funding

The author(s) declare financial support was received for the research, authorship, and/or publication of this article. This work was supported by the National Natural Science Foundation of China Grant 41974188, and the project was supported by the Specialized Research Fund for State Key Laboratories.

Acknowledgments

The authors acknowledge the Van Allen Probe team for the usage of the Van Allen Probe data. The authors would like to thank NASA's Space Physics Data Facility (SPDF) for providing the Van Allen Probe data and the solar wind parameters and geomagnetic indices.

Conflict of interest

The authors declare that the research was conducted in the absence of any commercial or financial relationships that could be construed as a potential conflict of interest.

Publisher's note

Supplementary material

The Supplementary Material for this article can be found online at: https://www.frontiersin.org/articles/10.3389/fspas.2024.1381764/full#supplementary-material

References

Allison, H. J., and Shprits, Y. Y. (2020). Local heating of radiation belt electrons to ultra-relativistic energies. *Nat. Coms.* 11 (1), 4533. doi:10.1038/s41467-020-18053-z

Allison, H. J., Shprits, Y. Y., Zhelavskaya, I. S., Wang, D., and Smirnov, A. G. (2021). Gyroresonant wave-particle interactions with chorus waves during extreme depletions of plasma density in the Van Allen radiation belts. *Sci. Advan.* 7 (5), eabc0380. doi:10.1126/sciadv.abc0380

Anderson, B. J., and Hamilton, D. C. (1993). Electromagnetic ion cyclotron waves stimulated by modest magnetospheric compressions. *J. Geophys. Res.* 98 (A7), 11369–11382. doi:10.1029/93JA00605

Baker, D. N., Hoxie, V., Zhao, H., Jaynes, A. N., Kanekal, S., Li, X., et al. (2019). Multi-year measurements of radiation belt electrons: acceleration, transport, and loss. *J. Geophys. Res. Space Phys.* 124 (4), 2588–2602. doi:10.1029/2018JA026259

Baker, D. N., Jaynes, A. N., Li, X., Henderson, M. G., Kanekal, S. G., Reeves, G. D., et al. (2014). Gradual diffusion and punctuated phase space density enhancements of highly relativistic electrons: Van Allen Probes observations. *Geophys. Res. Lett.* 41 (5), 1351–1358. doi:10.1002/2013GL058942

Baker, D. N., Kanekal, S. G., Hoxie, V. C., Batiste, S., Bolton, M., Li, X., et al. (2012). The relativistic electron-proton telescope (REPT) instrument on board the Radiation Belt Storm Probes (RBSP) spacecraft: characterization of Earth's radiation belt high-energy particle populations. *Space Sci. Rev.* 179 (1–4), 337–381. doi:10.1007/s11214-012-9950-9

Baker, D. N., Li, X., Turner, N., Allen, J. H., Bargatze, L. F., Blake, J. B., et al. (1997). Recurrent geomagnetic storms and relativistic electron enhancements in the outer magnetosphere: ISTP coordinated measurements. *J. Geophys. Res.* 102 (A7), 14141–14148. doi:10.1029/97JA00565

Blake, J. B., Carranza, P. A., Claudepierre, S. G., Clemmons, J. H., Crain, W. R., Dotan, Y., et al. (2013). The magnetic electron Ion spectrometer (MagEIS) instruments aboard the radiation belt storm probes (RBSP) spacecraft. *Space Sci. Rev.* 179 (1–4), 383–421. doi:10.1007/s11214-013-9991-8

Cao, X., Ni, B., Summers, D., Bortnik, J., Tao, X., Shprits, Y. Y., et al. (2017). Bounce resonance scattering of radiation belt electrons by H^+ band EMIC waves. *J. Geophys. Res. Space Phys.* 122, 1702–1713. doi:10.1002/2016JA023607

Capannolo, L., Li, W., Ma, Q., Chen, L., Shen, X.-C., Spence, H. E., et al. (2019). Direct observation of subrelativistic electron precipitation potentially driven by EMIC waves. *Geophys. Res. Lett.* 46 (12), 12711–12721. doi:10.1029/2019GL084202

Carson, B. R., Rodger, C. J., and Clilverd, M. A. (2013). POES satellite observations of EMIC-wave driven relativistic electron precipitation during 1998–2010. *J. Geophys. Res. Space Phys.* 118, 232–243. doi:10.1029/2012JA017998

Chen, J., Tang, C., Chu, X., Wang, X., Su, Z., Ni, B., et al. (2023). A statistical study on the acceleration conditions of ultrarelativistic electrons in the Earth's outer radiation belt during geomagnetic storms. *J. Geophys. Res. Space Phys.* 128, e2023JA032024. doi:10.1029/2023JA032024

Clilverd, M. A., Duthie, R., Hardman, R., Hendry, A. T., Rodger, C. J., Raita, T., et al. (2015). Electron precipitation from EMIC waves: a case study from 31 May 2013. *J. Geophys. Res. Space Phys.* 120, 3618–3631. doi:10.1002/2015JA021090

Drozdov, A. Y., Aseev, N., Effenberger, F., Turner, D. L., Saikin, A., and Shprits, Y. (2019). Storm time depletions ofmulti-MeV radiation belt electronsobserved at different pitch angles. *J. Geophys. Res. Space Phys.* 124, 8943–8953. doi:10.1029/2019JA027332

Engebretson, M. J., Posch, J. L., Wygant, J. R., Kletzing, C. A., Lessard, M. R., Huang, C., et al. (2015). Van Allen Probes, NOAA, GOES, and ground observations of an intense EMIC wave event extending over 12h in magnetic local time. *J. Geophys. Res. Space Phys.* 120, 5465–5488. doi:10.1002/2015JA021227

Forsyth, C., Rae, I. J., Murphy, K. R., Freeman, M. P., Huang, C.-L., Spence, H. E., et al. (2016). What effect do substorms have on the content of the radiation belts? *J. Geophys. Res. Space Phys.* 121 (7), 6292–6306. doi:10.1002/2016JA022620

Gao, X., Li, W., Bortnik, J., Thorne, R. M., Lu, Q., Ma, Q., et al. (2015). The effect of different solar wind parameters upon significant relativistic electron flux dropouts in the magnetosphere. *J. Geophys. Res. Space Phys.* 120 (6), 4324–4337. doi:10.1002/2015JA021182

Gokani, S. A., Han, D.-S., Selvakumaran, R., and Pant, T. K. (2022). Dependence of radiation belt flux depletions at geostationary orbit on different solar drivers during intense geomagnetic storms. *Front. Astron. Space Sci.* 9, 952486. doi:10.3389/fspas.2022.952486

Gu, X., Xia, S., Fu, S., Xiang, Z., Ni, B., Guo, J., et al. (2020). Dynamic responses of radiation belt electron fluxes to magnetic storms and their correlations with magnetospheric plasma wave activities. *Astrophys. J.* 891 (2), 127. doi:10.3847/1538-4357/ab71fc

Hajra, R., Tsurutani, B. T., Echer, E., Gonzalez, W. D., and Santolik, O. (2015). Relativistic (E > 0.6, > 2.0, and >4.0 MeV) electron acceleration at geosynchronous orbit during high-intensity, long-duration, continuous AE activity (HILDCAA) events. *Astrophys. J.* 39 (1), 39. doi:10.1088/0004-637X/799/1/39

Hua, M., Bortnik, J., and Ma, D. (2023). Dependence of electron flux dropouts in the Earth's outer radiation belt on energy and driving parameters during geomagnetic storms. *J. Geophys. Res. Space Phys.* 128, e2023JA031882. doi:10.1029/2023JA031882

Hua, M., Bortnik, J., and Ma, Q. (2022). Upper limit of outer radiation belt electron acceleration driven by whistler-mode chorus waves. *Geophys. Res. Lett.* 49 (15), e2022GL099618. doi:10.1029/2022GL099618

Hudson, M. K., Baker, D. N., Goldstein, J., Kress, B. T., Paral, J., Toffoletto, F. R., et al. (2014). Simulated magnetopause losses and Van Allen Probe flux dropouts. *Geophys. Res. Lett.* 41, 1113–1118. doi:10.1002/2014GL059222

Jaynes, A. N., Ali, A. F., Elkington, S. R., Malaspina, D. M., Baker, D. N., Li, X., et al. (2018). Fast diffusion of ultrarelativistic electrons in the outer radiation belt: 17 March 2015 storm event. *Geophys. Res. Lett.* 45 (20), 10874–10882. doi:10.1029/2018GL079786

Kersten, T., Horne, R. B., Glauert, S. A., Meredith, N. P., Fraser, B. J., and Grew, R. S. (2014). Electron losses from the radiation belts caused by EMIC waves. *J. Geophys. Res. Space Phys.* 119, 8820–8837. doi:10.1002/2014JA020366

Kim, H.-J., and Chan, A. A. (1997). Fully adiabatic changes in storm-time relativistic electron fluxes. *J. Geophys. Res.* 102 (A10), 22107–22116. doi:10.1029/97JA01814

Kim, H.-J., Lyons, L., Pinto, V., Wang, C.-P., and Kim, K.-C. (2015). Revisit of relationship between geosynchronous relativistic electron enhancements and magnetic storms. *Geophys. Res. Lett.* 42 (15), 6155–6161. doi:10.1002/2015GL065192

Kim, K. C., Lee, D.-Y., Kim, H.-J., Lyons, L. R., Lee, E. S., Oztusc rk, M. K., and Choi, C. R. (2008). Numerical calculations of relativistic electron drift loss effect. *J. Geophys. Res.* 113, A09212. doi:10.1029/2007ja013011

Lei, L. J., M, X., G, X. D., F, S., Z, Q., Y, J., et al. (2023). Study on the scattering loss timescales induced by multi-band EMIC waves on radiation belts relativistic electrons. *Chin. J. Geophys. (in Chinese)* 66 (9), 3610–3622. doi:10.6038/cjg2022Q0816

Li, L. Y., Cao, J. B., Yang, J. Y., and Dong, Y. X. (2013). Joint responses of geosynchronous magnetic field and relativistic electrons to external changes in solar wind dynamic pressure and interplanetary magnetic field. *J. Geophys. Res. Space Phys.* 118, 1472–1482. doi:10.1002/jgra.50201

Li, L. Y., Cao, J. B., Zhou, G. C., and Li, X. (2009). Statistical roles of storms and substorms in changing the entire outer zone relativistic electron population. *J. Geophys. Res.* 114 (A12), A12214. doi:10.1029/2009JA014333

Li, L. Y., Yu, J., Cao, J. B., and Yuan, Z. G. (2016). Compression-amplified EMIC waves and their effects on relativistic electrons. *Phys. Plasmas.* 23, 062116. doi:10.1063/1.4953899

Li, W., Ma, Q., Thorne, R. M., Bortnik, J., Zhang, X. J., Li, J., et al. (2016). Radiation belt electron acceleration during the 17 March 2015 geomagnetic storm: observations and simulations. *J. Geophys. Res. Space Phys.* 121 (6), 5520–5536. doi:10.1002/2016JA022400

Li, W., Thorne, R. M., Bortnik, J., Baker, D. N., Reeves, G. D., Kanekal, S. G., et al. (2015). Solar wind conditions leading to efficient radiation belt electron acceleration: a superposed epoch analysis. *Geophys. Res. Lett.* 42 (17), 6906–6915. doi:10.1002/2015GL065342

Li, W., Thorne, R. M., Ma, Q., Ni, B., Bortnik, J., Baker, D. N., et al. (2014). Radiation belt electron acceleration by chorus waves during the 17 March 2013 storm. *J. Geophys. Res. Space Phys.* 119 (6), 4681–4693. doi:10.1002/2014JA019945

Li, X., Baker, D. N., Temerin, M., Cayton, T. E., Reeves, E. G. D., Christensen, R. A., et al. (1997). Multisatellite observations of the outer zone electron variation during the November 3–4, 1993, magnetic storm. *J. Geophys. Res.* 102 (A7), 14123–14140. doi:10.1029/97JA01101

Loto'aniu, T. M., Singer, H. J., Waters, C. L., Angelopoulos, V., Mann, I. R., Elkington, S. R., et al. (2010). Relativistic electron loss due to ultralow frequency waves and enhanced outward radial diffusion. *J. Geophys. Res.* 115, A12245. doi:10.1029/2010JA015755

Ma, Q., Li, W., Thorne, R. M., Nishimura, Y., Zhang, X. J., Reeves, G. D., et al. (2016). Simulation of energy-dependent electron diffusion processes in the Earth's outer radiation belt. *J. Geophys. Res. Space Phys.* 121 (5), 4217–4231. doi:10.1002/2016JA022507

McCollough, J. P., Elkington, S. R., Usanova, M. E., Mann, I. R., Baker, D. N., and Kale, Z. C. (2010). Physical mechanisms of compressional EMIC wave growth. *J. Geophys. Res.* 115 (A10), A10214. doi:10.1029/2010JA015393

Meredith, N. P., Thorne, R. M., Horne, R. B., Summers, D., Fraser, B. J., and Anderson, R. R. (2003). Statistical analysis of relativistic electron energies for cyclotron resonance with EMIC waves observed on CRRES. *J. Geophys. Res.* 108 (A6), 1250. doi:10.1029/2002JA009700

Miyoshi, Y., Sakaguchi, K., Shiokawa, K., Evans, D., Albert, J., Connors, M., et al. (2008). Precipitation of radiation belt electrons by EMIC waves, observed from ground and space. *Geophys. Res. Lett.* 35, L23101. doi:10.1029/2008GL035727

Mourenas, D., Artemyev, A. V., Ma, Q., Agapitov, O. V., and Li, W. (2016). Fast dropouts of multi-MeV electrons due to combined effects of EMIC and whistler-mode waves. *Geophys. Res. Lett.* 43, 4155–4163. doi:10.1002/2016GL068921

Moya, P. S., Pinto, V. A., Sibeck, D. G., Kanekal, S. G., and Baker, D. N. (2017). On the effect of geomagnetic storms on relativistic electrons in the outer radiation belt: Van Allen Probes observations. *J. Geophys. Res. Space Phys.* 122 (11), 11100–11108. doi:10.1002/2017JA024735

Ni, B., Cao, X., Shprits, Y. Y., Summers, D., Gu, X., Fu, S., et al. (2018). Hot plasma effects on the cyclotron-resonant pitch-angle scattering rates of radiation belt electrons due to EMIC waves. *Geophys. Res. Lett.* 45, 21–30. doi:10.1002/2017GL076028

Ni, B., Cao, X., Zou, Z., Zhou, C., Gu, X., Bortnik, J., et al. (2015). Resonant scattering of outer zone relativistic electrons by multi-band EMIC waves and resultant electron loss time scales. *J. Geophys. Res. Space Phys.* 120, 7357–7373. doi:10.1002/2015JA021466

Onsager, T. G., Green, J. C., Reeves, G. D., and Singer, H. J. (2007). Solar wind and magnetospheric conditions leading to the abrupt loss of outer radiation belt electrons. *J. Geophys. Res.* 112 (A1), A01202. doi:10.1029/2006JA011708

Reeves, G. D. (1998). Relativistic electrons and magnetic storms: 1992–1995. *Geophys. Res. Lett.* 25 (11), 1817–1820. doi:10.1029/98GL01398

Reeves, G. D., McAdams, K. L., Friedel, R. H. W., and O'Brien, T. P. (2003). Acceleration and loss of relativistic electrons during geomagnetic storms. *Geophys. Res. Lett.* 30 (10), 1529. doi:10.1029/2002GL016513

Reeves, G. D., Morley, S. K., Friedel, R. H., Henderson, M. G., Cayton, T. E., Cunningham, G., et al. (2011). On the relationship between relativistic electron flux and solar wind velocity: paulikas and Blake revisited. *J. Geophys. Res.* 116 (A2), A02213. doi:10.1029/2010JA015735

Reeves, G. D., Spence, H. E., Henderson, M. G., Morley, S. K., Friedel, R. H. W., Funsten, H. O., et al. (2013). Electron acceleration in the heart of the Van Allen radiation belts. *Science* 341 (6149), 991–994. doi:10.1126/science.1237743

Rodger, C. J., Hendry, A. T., Clilverd, M. A., Kletzing, C. A., Brundell, J. B., and Reeves, G. D. (2015). High-resolution *in situ* observations of electron precipitation-causing EMIC waves. *Geophys. Res. Lett.* 42, 9633–9641. doi:10.1002/2015GL066581

Saikin, A. A., Zhang, J.-C., Smith, C. W., Spence, H. E., Torbert, R. B., and Kletzing, C. A. (2016). The dependence on geomagnetic conditions and solar wind dynamic pressure of the spatial distributions of EMIC waves observed by the Van Allen Probes. *J. Geophys. Res. Space Phys.* 121, 4362–4377. doi:10.1002/2016JA022523

Schiller, Q., Li, X., Blum, L., Tu, W., Turner, D. L., and Blake, J. B. (2014). A nonstorm time enhancement of relativistic electrons in the outer radiation belt. *Geophys. Res. Lett.* 41 (1), 7–12. doi:10.1002/2013GL058485

Shprits, Y., Daae, M., and Ni, B. (2012). Statistical analysis of phase space density buildups and dropouts. *J. Geophys. Res.* 117, A01219. doi:10.1029/2011JA016939

Shprits, Y. Y., Allison, H. J., Wang, D., Drozdov, A., Szabo-Roberts, M., Zhelavskaya, I., et al. (2022). A new population of ultra-relativistic electrons in the outer radiation zone. *J. Geophys. Res. Space Phys.* 127 (5), e2021JA030214. doi:10.1029/2021JA030214

Shprits, Y. Y., Drosdov, A. Y., Spasojevic, M., Kellerman, A. C., Usanova, M. E., Engebretson, M. J., et al. (2016). Wave-induced loss of ultra-relativistic electrons in the Van Allen radiation belts. *Nat. Com* 7, 12883. doi:10.1038/ncomms12883

Shprits, Y. Y., Subbotin, D., Drozdov, A., Usanova, M. E., Kellerman, A., Orlova, K., et al. (2013). Unusual stable trapping of the ultrarelativistic electrons in the Van Allen radiation belts. *Nat. Phys.* 9, 699–703. doi:10.1038/nphys2760

Shprits, Y. Y., Thorne, R. M., Friedel, R., Reeves, G. D., Fennell, J., Baker, D. N., et al. (2006). Outward radial diffusion driven by losses at magnetopause. *J. Geophys. Res.* 111 (A11). doi:10.1029/2006JA011657

Spence, H. E., Reeves, G. D., Baker, D. N., Blake, J. B., Bolton, M., Bourdarie, S., et al. (2013). Science goals and overview of the Radiation Belt Storm Probes (RBSP) energetic particle, composition, and thermal plasma (ECT) suite on NASA's Van Allen probes mission. *Space Sci. Rev.* 179 (1–4), 311–336. doi:10.1007/s11214-013-0007-5

Staples, F. A., Ma, Q., Kellerman, A., Rae, I. J., Forsyth, C., Sandhu, J. K., et al. (2023). Differentiating between simultaneous loss drivers in Earth's outer radiation belt: multi-dimensional phase space density analysis. *Geophys. Res. Lett.* 50, e2023GL106162. doi:10.1029/2023GL106162

Su, Z., Gao, Z., Zheng, H., Wang, Y., Wang, S., Spence, H. E., et al. (2017). Rapid loss of radiation belt relativistic electrons by EMIC waves. *J. Geophys. Res. Space Phys.* 122, 9880–9897. doi:10.1002/2017JA024169

Su, Z., Gao, Z., Zhu, H., Li, W., Zheng, H., Wang, Y., et al. (2016). Nonstorm time dropout of radiation belt electron fluxes on 24 September 2013. *J. Geophys. Res. Space Phys.* 121, 6400–6416. doi:10.1002/2016JA022546

Su, Z. P., Zhu, H., Xiao, F. L., Zheng, H. N., Wang, Y. M., Zong, Q.-G., et al. (2014). Quantifying the relative contributions of substorm injections and chorus waves to the rapid outward extension of electron radiation belt. *J. Geophys. Res. Space Phys.* 119 (12), 10023–10040. doi:10.1002/2014JA020709

Su, Z. P., Zhu, H., Xiao, F. L., Zong, Q.-G., Zhou, X.-Z., Zheng, H., et al. (2015). Ultra-low-frequency wave-driven diffusion of radiation belt relativistic electrons. *Nat. Com* 6 (1), 10096. doi:10.1038/ncomms10096

Summers, D., Ni, B., and Meredith, N. P. (2007). Timescales for radiation belt electron acceleration and loss due to resonant wave-particle interactions: 2. Evaluation for VLF chorus, ELF hiss, and electromagnetic ion cyclotron waves. *J. Geophys. Res.* 112 (A4), A04207. doi:10.1029/2006JA011993

Tang, C., Yang, C., Chen, J., Wang, X., Ni, B., Su, Z., et al. (2023a). Rapid enhancements of relativistic electrons in the Earth's outer radiation belt caused by the intense substorms: a statistical study. *J. Geophys. Res. Space Phys.* 128, e2022JA031089. doi:10.1029/2022JA031089

Tang, C. L., Su, Z. P., Ni, B. B., Zhang, J. C., Chen, J. R., and Wang, X. (2023b). The effects of geomagnetic activities on acceleration regions of radiation belt electrons. *J. Geophys. Res. Space Phys.* 128 (6), e2022JA031229. doi:10.1029/2022JA031229

Tang, C. L., Wang, Y. X., Ni, B. B., Su, Z. P., Reeves, G. D., Zhang, J.-C., et al. (2017). The effects of magnetospheric processes on relativistic electron dynamics in the Earth's outer radiation belt. *J. Geophys. Res. Space Phys.* 122 (10), 9952–9968. doi:10.1002/2017JA024407

Tang, C. L., Zhang, J.-C., Reeves, G. D., Su, Z. P., Baker, D. N., Spence, H. E., et al. (2016). Prompt enhancement of the Earth's outer radiation belt due to substorm electron injections. *J. Geophys. Res. Space Phys.* 121 (12), 11826–11838. doi:10.1002/2016JA023550

Thorne, R. M., Li, W., Ni, B., Ma, Q., Bortnik, J., Chen, L., et al. (2013). Rapid local acceleration of relativistic radiation belt electrons by magnetospheric chorus. *Nature* 504 (7480), 411–414. doi:10.1038/nature12889

Turner, D. L., Angelopoulos, V., Li, W., Bortnik, J., Ni, B., Ma, Q., et al. (2014). Competing source and loss mechanisms due to wave-particle interactions in Earth's outer radiation belt during the 30 September to 3 October 2012 geomagnetic storm. *J. Geophys. Res. Space Phys.* 119, 1960–1979. doi:10.1002/2014JA019770

Turner, D. L., Kilpua, E. K. J., Hietala, H., Claudepierre, S. G., O'Brien, T. P., Fennell, J. F., et al. (2019). The response of Earth's electron radiation belts to geomagnetic storms: statistics from the Van Allen Probes era including effects from different storm drivers. *J. Geophys. Res. Space Phys.* 124 (2), 1013–1034. doi:10.1029/2018JA026066

Turner, D. L., O'Brien, T. P., Fennell, J. F., Claudepierre, S. G., Blake, J. B., Kilpua, E. K. J., et al. (2015). The effects of geomagnetic storms on electrons in earth's radiation belts. *Geophys. Res. Lett.* 42 (21), 9176–9184. doi:10.1002/2015GL064747

Turner, D. L., Shprits, Y., Hartinger, M., and Angleopoulos, V. (2012). Explaining sudden losses of outer radiation belt electrons during geomagnetic storms. *Nat. Phys.* 8, 208–212. doi:10.1038/nphys2185

Ukhorskiy, A. Y., and Sitnov, M. I. (2008). Radial transport in the outer radiation belt due to global magnetospheric compressions. *J. Atmos. Sol.-Terr. Phys.* 70, 1714–1726. doi:10.1016/j.jastp.2008.07.018

Usanova, M. E., Drozdov, A., Orlova, K., Mann, I. R., Shprits, Y., Robertson, M. T., et al. (2014). Effect of EMIC waves on relativistic and ultrarelativistic electron populations: ground-based and Van Allen Probes observations. *Geophys. Res. Lett.* 41, 1375–1381. doi:10.1002/2013GL059024

Usanova, M. E., Mann, I. R., Bortnik, J., Shao, L., and Angelopoulos, V. (2012). THEMIS observations of electromagnetic ion cyclotron wave occurrence: dependence on AE, SYMH, and solar wind dynamic pressure. *J. Geophys. Res.* 117, A10218. doi:10.1029/2012JA018049

Wang, X., Tang, C., Ni, B., Su, Z., Zhang, J., Chen, J., et al. (2023). The evolutions of the seed and relativistic electrons in the Earth's outer radiation belt during the geomagnetic storms: a statistical study. *J. Geophys. Res. Space Phys.* 128 (5), e2023JA031284. doi:10.1029/2023JA031284

Wing, S., Johnson, J. R., Camporeale, E., and Reeves, G. D. (2016). Information theoretical approach to discovering solar wind drivers of the outer radiation belt. *J. Geophys. Res. Space Phys.* 121 (10), 9378–9399. doi:10.1002/2016JA022711

Xiang, Z., Ni, B., Zhou, C., Zou, Z., Gu, X., Zhao, Z., et al. (2016). Multi-satellite simultaneous observations of magnetopause and atmospheric losses of radiation belt electrons during an intense solar wind dynamic pressure pulse. *Ann. Geophys.* 34, 493–509. doi:10.5194/angeo-34-493-2016

Xiang, Z., Tu, W., Ni, B., Henderson, M. G., and Cao, X. (2018). A statistical survey of radiation belt dropouts observed by Van Allen Probes. *Geophys. Res. Lett.* 45, 8035–8043. doi:10.1029/2018GL078907

Xue, Z., Yuan, Z., Yu, X., Huang, Z., and Deng, D. (2023). Enhanced solar wind dynamic pressure as a driver of low-energy proton temperature anisotropies and high-frequency EMIC waves. *J. Geophys. Res. Space Phys.* 128, e2023JA031929. doi:10.1029/2023JA031929

Yahnin, A. G., and Yahnina, T. A. (2022). 1 MeV electron dynamics in the outer radiation belt during geomagnetic storms on september 7–8, 2017. *Bull. Russ. Acad. Sci. Phys.* 86, 275–280. doi:10.3103/S1062873822030273

Yahnin, A. G., Yahnina, T. A., Raita, T., and Manninen, J. (2017). Ground pulsation magnetometer observations conjugated with relativistic electron precipitation. *J. Geophys. Res. Space Physics* 122, 9169–9182. doi:10.1002/2017JA024249

Yan, Y., Yue, C., Yin, Z.-F., Zhou, X.-Z., Zong, Q.-G., and Li, J.-H. (2023). Amplitude-dependent properties and excitation mechanisms of EMIC waves in

the Earth's inner magnetosphere. *J. Geophys. Res. Space Phys.* 128, e2023JA031451. doi:10.1029/2023JA031451

Yuan, C., and Zong, Q. (2013). Relativistic electron fluxes dropout in the outer radiation belt under different solar wind conditions. *J. Geophys. Res. Space Phys.* 118 (12), 7545–7556. doi:10.1002/2013JA019066

Yuan, Z., Liu, K., Yu, X., Yao, F., Huang, S., Wang, D., et al. (2018). Precipitation of radiation belt electrons by EMIC waves with conjugated observations of NOAA and Van Allen satellites. *Geophys. Res. Lett.* 45 (12), 694–702. doi:10.1029/2018GL080481

Zhang, X.-J., Li, W., Ma, Q., Thorne, R. M., Angelopoulos, V., Bortnik, J., et al. (2016a). Direct evidence for EMIC wave scattering of relativistic electrons in space. *J. Geophys. Res. Space Phys.* 121, 6620–6631. doi:10.1002/2016JA022521

Zhang, X.-J., Li, W., Thorne, R. M., Angelopoulos, V., Bortnik, J., Kletzing, C. A., et al. (2016b). Statistical distribution of EMIC wave spectra: observations from van allen probes. *Geophys. Res. Lett.* 43 (12), 348–355. doi:10.1002/2016GL071158

Zhang, X.-J., Mourenas, D., Shen, X.-C., Qin, M., Artemyev, A. V., Ma, Q., et al. (2021). Dependence of relativistic electron precipitation in the ionosphere on EMIC wave minimum resonant energy at the conjugate equator. *J. Geophys. Res. Space Phys.* 126, e2021JA029193. doi:10.1029/2021JA029193

Zhao, H., Baker, D. N., Jaynes, A. N., Li, X., Elkington, S. R., Kanekal, S. G., et al. (2017). On the relation between radiation belt electrons and solar wind parameters/geomagnetic indices: dependence on the first adiabatic invariant and L. *J. Geophys. Res. Space Phys.* 122 (2), 1624–1642. doi:10.1002/2016JA023658

Zhao, H., Baker, D. N., Li, X., Jaynes, A. N., and Kanekal, S. G. (2018). The acceleration of ultrarelativistic electrons during a small to moderate storm of 21 April 2017. *Geophys. Res. Lett.* 45 (12), 5818–5825. doi:10.1029/2018GL078582

Zhao, H., Baker, D. N., Li, X., Jaynes, A. N., and Kanekal, S. G. (2019a). The effects of geomagnetic storms and solar wind conditions on the ultrarelativistic electron flux enhancements. *J. Geophys. Res. Space Phys.* 124 (3), 1948–1965. doi:10.1029/2018JA026257

Zhao, H., Johnston, W. R., Baker, D. N., Li, X., Ni, B., Jaynes, A. N., et al. (2019b). Characterization and evolution of radiation belt electron energy spectra based on the Van Allen Probes measurements. *J. Geophys. Res. Space Phys.* 124 (6), 4217–4232. doi:10.1029/2019JA026697

Zhu, H., and Chen, L. (2019). On the observation of electrostatic harmonics associated with EMIC waves. *Geophys. Res. Lett.* 46, 14274–14281. doi:10.1029/2019gl085528

Zhu, H., Chen, L., Claudepierre, S. G., and Zheng, L. (2020). Direct evidence of the pitch angle scattering of relativistic electrons induced by EMIC waves. *Geophys. Res. Lett.* 47, e2019GL085637. doi:10.1029/2019GL085637